

Compact Modeling of High Frequency Phenomena for On-Chip Spiral Inductors (Invited Paper)

Niranjan Talwalkar¹, C. Patrick Yue², S. Simon Wong³

¹Center for Integrated Systems, Stanford University, CA, USA, narya@stanford.edu

²Aeluros Inc., Mountain View, CA, USA, patrick@aeluros.com

³Center for Integrated Systems, Stanford University, CA, USA, wong@ee.stanford.edu

ABSTRACT

This paper presents a physics-based compact model for predicting high frequency performance of spiral inductors. The model accurately accounts for skin effect and proximity effect in the metal conductors as well as eddy current loss in the silicon substrate at high frequencies. Skin effect is modeled accurately up to 20 GHz using a reduced partial element equivalent circuit formulation (PEEC). Proximity effect in multi-turn inductors is modeled using an “effective width” approach. Substrate eddy current is modeled with an effective substrate image current profile, which accounts for dependence on substrate resistivity, oxide thickness, and inductor trace width. The model shows excellent agreements with measured data across a variety of inductor geometries and substrate resistivities up to 20 GHz. This model can be applied to modeling on-chip coplanar lines at high frequencies.

Keywords: On-chip inductors, coplanar lines, pskin effect, proximity effect, substrate eddy current loss.

INTRODUCTION

Advanced CMOS and SiGe technologies have made RF applications up to 10 GHz practical [1][2]. While passives, such as spiral inductors and coplanar lines, are key to these designs, their high-frequency behaviors are not well understood or modeled. Several phenomena degrades the performance of on-chip passives at high frequencies including skin effect, proximity effect, electric field penetration into substrate, and substrate eddy current losses. Due to the complexity of the electromagnetics in an inductor, analytical solutions are not known to exist. Fullwave 3D simulations are quite slow and hence not useful for circuit designers. Using the PEEC formulation [5], techniques have been developed for estimating skin, proximity, and substrate effects [6]-[7]. However, synthesis and optimization using these methods will be computationally excessive. Compact expressions for skin effect proposed in [8] are quite suitable for typical interconnect geometries but not for inductors which tends to

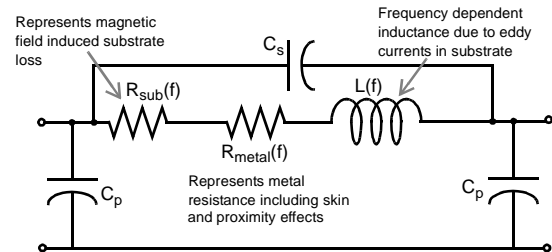


Figure 1: Equivalent circuit for spiral inductor with PGS.

have wide ($\sim 10 \mu\text{m}$) metal traces. The compact model for proximity effect proposed by Kuhn in [9] is found to be valid only for limited frequencies. The loss due to electric field penetration in the substrate can be modeled as described in [3] and eliminated using a properly designed patterned ground shield (PGS) [4]. Hasegawa [10] predicted that the eddy current loss for lines over doped substrates assuming certain modes of operation. However, today’s wireless applications operate at frequencies which are in between the asymptotic frequency limits based on Hasegawa’s model. This paper presents a physics-based compact model which accurately predicts these high-frequency effects while providing design insight for optimizing inductor design.

MODEL DEVELOPMENT

2.1 Skin Effect

Skin effect is modeled here using a modified PEEC approach by dividing the conductor cross-section into multiple segments. It is observed that 6 segments, with different widths, provide sufficient accuracy to model ac current redistribution (Figure 2). Each segment is assumed to have no lateral current redistribution but can have a vertical current non-uniformity. This vertical current non-uniformity results in an increase in ac resistance given by Eq. 1, where ‘ t ’ is thickness of the conductor and ‘ δ ’ is the skin depth in the metal.

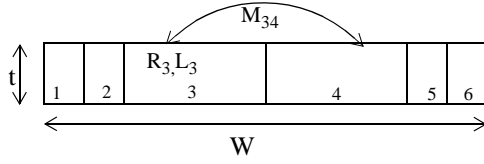


Figure 2: Modeling skin effect in rectangular conductors.

$$\frac{R_{vertical}(f)}{R_{dc}} = Real\left(\left(\frac{\gamma}{2}\right) \cosh\left(\frac{\gamma}{2}\right)\right) \quad \gamma = \frac{(1+j)}{\delta} \quad (1)$$

The symmetry of the skin effect problem allows the number of equations to be reduced from six to three. The resulting problem is formulated in Eq. 2 which has a compact solution with sufficient accuracy up to 20 GHz. Self and mutual inductances used in Eq. 2 are computed using the formulae by Greenhouse [12]. R_1 , R_2 and R_3 , the resistances associated with the different segments, which are inputs for Eq. 2, are calculated as a thickness dependent value given by Eq. 1.

$$\begin{bmatrix} V \\ V \\ V \end{bmatrix} = \begin{bmatrix} R_1 + j\omega(L_1 + M_{16}) & j\omega(M_{12} + M_{15}) & j\omega(M_{13} + M_{14}) \\ j\omega(M_{12} + M_{15}) & R_2 + j\omega(L_2 + M_{25}) & j\omega(M_{23} + M_{24}) \\ j\omega(M_{13} + M_{14}) & j\omega(M_{23} + M_{24}) & R_3 + j\omega(L_3 + M_{34}) \end{bmatrix} \begin{bmatrix} I_1 \\ I_2 \\ \frac{I_1 - I_2}{2} \end{bmatrix} \quad (2)$$

$$R_{metal}(f) = Real\left(\frac{V}{I}\right)$$

2.2 Proximity Effect

Proximity effects in inductors are due to conductors carrying currents in the same as well as opposite directions as shown in Figure 3.

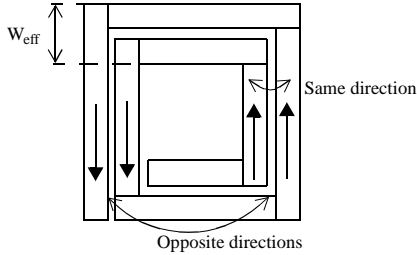


Figure 3: Modeling proximity effects in the spiral inductor.

Typical inductor designs are hollow [11], therefore the proximity effect between conductors carrying current in the opposite direction is negligible. The proximity effect between the closely spaced conductors carrying currents in the same direction is estimated by treating these conductors as a single conductor of width “ W_{eff} ”. The ac resistance increase is then estimated using the skin effect calculation for this wide conductor as shown in Section 2.1. As will be verified in Section 3.1, this assumption is reasonable in most inductor designs where the width of each line is much greater than the spacing between the lines.

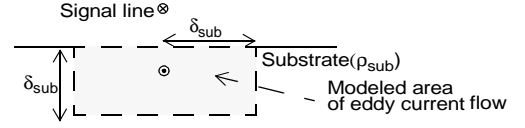


Figure 4: Modeling of the substrate current distribution.

2.3 Effect of Eddy Current in the Substrate

Time-varying magnetic fields penetrate the silicon substrate and cause eddy currents as per Lenz’s law. These eddy currents cause power loss as well as inductance reduction. For modeling purposes, eddy current substrate losses are first derived for coplanar lines and the results are extended to model loss for the inductor. The substrate loss model presented here is based on three key points:

- Every signal line has an image substrate current whose magnitude is equal to that of the signal current.
- The substrate current distribution is approximated as a uniform current density, J_{avg} , with a rectangular cross-section of dimensions, “ δ_{sub} ” (Figure 4). Since the real current flow cross-section is non-rectangular, the parameter “ α ” is introduced to account for the rectangular approximation (Eq. 3).

$$I_{sub} = \int J_{sub}(x,y) dx dy = \alpha J_{avg} \int_{-\delta_{sub}}^{\delta_{sub}} \int_{-\delta_{sub}}^{\delta_{sub}} dx dy = 2\alpha J_{avg} \delta_{sub}^2 \quad (3)$$

- The net substrate current due to multiple interconnect lines is calculated by superposition.

2.3.1 Coplanar Transmission Line

Modeled current profiles for a coplanar transmission line under three different geometric conditions are shown in Figure 5. Using these profiles and substrate doping, the power loss and hence R_{sub} (Eq. 4) per unit length can be computed for the coplanar line. Eddy current loss dependence on signal line width, given by β (Eq. 5), is derived by dividing the line into infinitesimal pieces and superposing the substrate current corresponding to each of them. Dependence on the height above the lossy substrate layer is accounted for by η (Eq. 6).

$$R_{sub} = \begin{cases} \frac{\beta \eta \rho_{sub}}{2} & P > 2\delta_{sub} \\ \frac{\beta \eta P \rho_{sub}}{4\alpha \delta_{sub}^3} & P < 2\delta_{sub} < 2t_{sub} \\ \frac{\beta \eta P t_{sub} \rho_{sub}}{4\alpha \delta_{sub}^4} & 2t_{sub} < 2\delta_{sub} \end{cases} \quad (4)$$

$$\beta = \begin{cases} 1 - \frac{W}{6\delta_{sub}} & P > 2\delta_{sub}, W < 2\delta_{sub} \\ \frac{2\delta_{sub}(W - \frac{2}{3}\delta_{sub})}{W^2} & P > 2\delta_{sub}, W > 2\delta_{sub} \\ 1 - \frac{W}{3P} & P < 2\delta_{sub} \end{cases} \quad (5)$$

$$\eta = \left(1 - \frac{2h}{\sqrt{P^2 + (2h)^2}}\right) \quad (6)$$

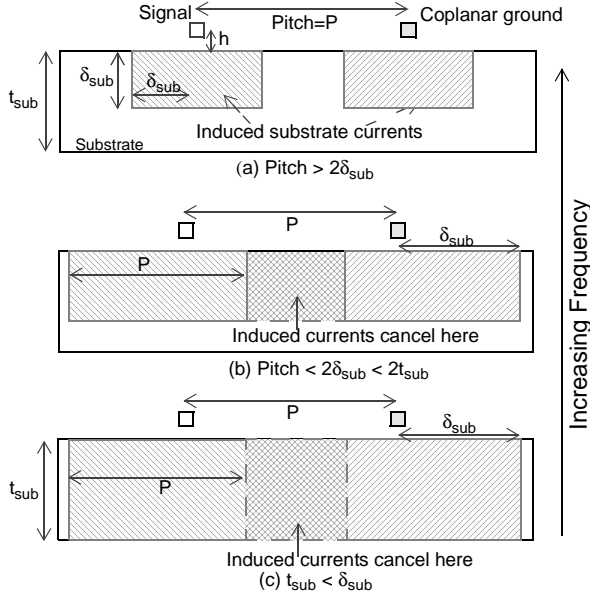


Figure 5: Coplanar transmission line modeling.

Note that Eq. 4 agrees with predictions of [10] in the slow-wave and skin-effect modes. Based on the current distributions in the substrate, the mutual inductance between signal lines and eddy currents can be calculated using the formulae by Greenhouse [12]. The net inductance of the signal lines is calculated in Eq. 7, where L_{int} is the dc value of the interconnect inductance and $M_{int-sub}$ is the mutual coupling between the interconnect and the substrate.

$$L(f) = L_{int} - M_{int-sub}(f) \quad (7)$$

2.3.2 Spiral Inductor

Eddy current loss for a single turn inductor is calculated by treating it as a sum of the losses of two orthogonal coplanar lines (Figure 6). Furthermore, a multiturn inductor can be modeled as a single turn inductor with “N” parallel conducting segments. R_{sub} from Eq. 4 scales by “ N^2 ” to account for the effects of superposition of the N turns. Also, the pitch is replaced by D_{avg} , the average diameter for the inductor.

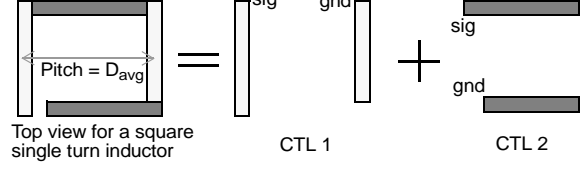


Figure 6: Modeling substrate loss for a single-turn inductor. For a multiturn inductor, the frequency dependent inductance is obtained from Eq. 8, where L_s is the low frequency inductance of the spiral found from Greenhouse formulae [12] and ‘ $M_{ind-sub}$ ’ is the mutual inductance between the spiral and the substrate by treating the spiral as a single turn inductor of width ‘ W_{eff} ’. ‘ N^2 ’ accounts for the composite coupling of the substrate current to the N turns of the spiral.

$$L(f) = L_s - N^2 M_{ind-sub}(f) \quad (8)$$

MODEL VERIFICATION

The proposed model was evaluated by comparison with 2-D simulations (using Maxwell™ [13], a fullwave electromagnetic simulator) and experiments.

3.1 Simulation Results

Skin and proximity effect models were compared to 2-D simulation results from Maxwell™ (Figure 7). The strong width dependence of skin effect is captured well by the model. It is also verified that for multiple signal lines ($W_1=W_2=15\mu\text{m}$; $W_{eff}=30\mu\text{m}$) separated by a short distance ($1\mu\text{m}$), the composite impact of skin and proximity effect is the same as the impact of only skin effect on a signal line of the same effective width ($W=30\mu\text{m}$).

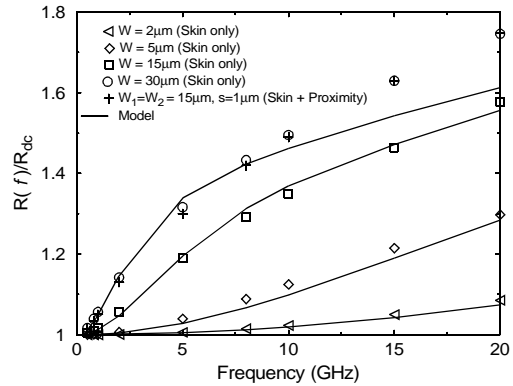


Figure 7: Width dependence of skin and proximity effects ($t=1\mu\text{m}$, $\text{Al } \sigma=3.8e7$)

3.2 Measurement Results

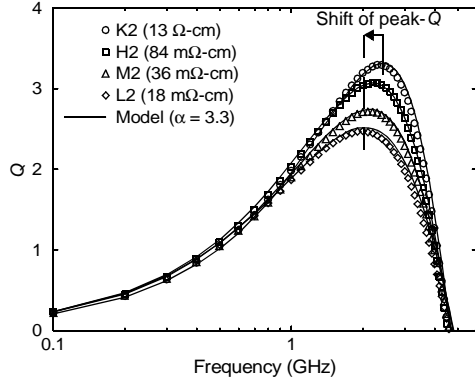


Figure 8: Impact of substrate doping on Q ($D_{out}=250\mu\text{m}$, $W=3.3\mu\text{m}$, $N_{\text{turns}}=4$, $L_{dc} = 7.88\text{nH}$)

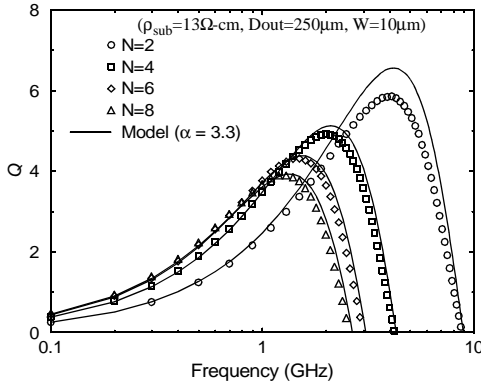


Figure 9: Model performance for different number of turns for a lightly doped substrate.

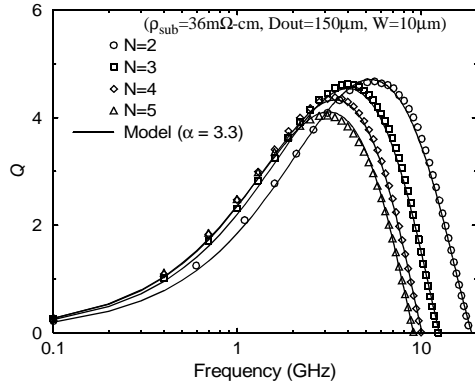


Figure 10: Model performance for different number of turns for a heavily doped substrate.

Inductors of various dimensions were fabricated in a 3-metal back-end process on substrates of five different resistivities; $13\Omega\text{-cm}$, $0.64\text{m}\Omega\text{-cm}$, $84\text{m}\Omega\text{-cm}$, $36\text{m}\Omega\text{-cm}$, and $18\text{m}\Omega\text{-cm}$. All structures had PGSSs to prevent electric field penetration into the substrate. $1.6\mu\text{m}$ thick Al was used as metal conductor with $1\mu\text{m}$ SiO_2 as the insulator.

One-port S-parameters were measured with a HP8510 Network Analyzer using techniques presented in [3]. The equivalent circuit of Figure 1 was used with one of the ports shorted out. Figure 8 shows the large dependence of the quality factor (Q^1) on substrate doping. Note that the peak Q occurs at different frequencies depending on the substrate doping. Figure. 9 shows that the model behaves well with respect to geometry for a lightly doped substrate where skin and proximity effects are dominant. In Figure 10, the model is verified for different geometries in a heavily doped substrate where eddy current effects dominate. For the most part, the model error across all the substrates and inductor geometries (150 samples) was found to be less than 10%. These errors include those due to process variations and measurements. Note that a single fitting parameter, $\alpha = 3.3$, models the loss for all geometries and substrate dopings.

REFERENCES

- [1] H. Cong et al., "A 10Gb/s 16:1 multiplexer and 10GHz clock synthesizer in $0.25\mu\text{m}$ SiGe BiCMOS," *ISSCC 2001*, pp. 80-81, Feb 2001.
- [2] B. Kleveland et al., "Monolithic CMOS distributed amplifier and oscillator," *ISSCC 1999*, pp. 70-71, Feb 1999.
- [3] C.P. Yue et al., "A physical model for planar spiral inductors on silicon," *IEDM Tech. Dig.*, pp. 155-158, Dec 1996.
- [4] C.P. Yue and S.S. Wong, "On-chip spiral inductors with patterned ground shields for Si-based RF ICs," *IEEE JSSC*, Vol. 33, no. 5, pp.743-752, May 1998.
- [5] A.E. Ruehli and H. Heeb, "Circuit models for three-dimensional geometries including dielectrics", *IEEE Transaction on Microwave Theory and Techniques*, Vol. 40, pp. 1507-1516, July 1992.
- [6] A.M. Niknejad and R.G. Meyer, "Analysis of eddy-current losses over conductive substrates with applications to monolithic inductors and transformers," *IEEE Transactions on Microwave Theory and Techniques*, Vol. 49, No. 1, 166-176, Jan 2001.
- [7] Y. Massoud and J. White, "Simulation and modeling of effect of substrate conductivity on coupling inductance," *IEDM 95*, pp. 491-494, Dec 1995.
- [8] Pettenpaul et al. , "CAD models of Lumped Elements on GaAs up to 18 GHz," *IEEE Transactions on Microwave Theory and Techniques*, Vol. 36, No. 2, Feb 1988.
- [9] W.B. Kuhn et al., "Analysis of Current Crowding Effects in Multiturn Spiral Inductors," *IEEE Trans. MTTs*, Vol. 49, No. 1, January 2001.
- [10] H. Hasegawa et al., "Properties of Microstrip Line on Si-SiO₂ System," *IEEE Trans. MTTs*, Vol. 19, No. 11 November 1971.
- [11] J. Craninckx and M. Steyaert, "A 1.8-GHz low-phase-noise CMOS VCO using optimized hollow spiral inductors", *IEEE J. Solid-State Circuits*, Vol. 32, pp. 736-745, May 1997.
- [12] H.M. Greenhouse, "Design of planar rectangular microelectronic inductors," *IEEE Transactions on Parts, Hybrids, and Packaging*, Vol. PHP-10, No. 2, pp. 101-109, June 1974.
- [13] *Maxwell 2D Parameter Extractor User's Reference*, Ansoft Corporation, 2001.

1. Q-factor is defined as $\text{Imag}(Z_{in})/\text{Real}(Z_{in})$